Available online at www.sciencedirect.com
SCIENCE DIRECT®
Journal of Hydrology 280 (2003) 207–228
Journal of Hydrology
www.elsevier.com/locate/jhydrol

Development of a high resolution runoff routing model, calibration and application to assess runoff from the LMD GCM

Agnès Ducharne[a,d,*], Catherine Golaz[b], Etienne Leblois[c], Katia Laval[a], Jan Polcher[a], Emmanuel Ledoux[b], Ghislain de Marsily[d]

[a]*Laboratoire de Météorologie Dynamique du CNRS, Université Pierre et Marie Curie, Paris, France*
[b]*Laboratoire CNRS Sisyphe, Centre d'Informatique Géologique, ENSMP, Fontainebleau, France*
[c]*Cemagref, Lyon, France*
[d]*Laboratoire CNRS Sisyphe, Université Pierre et Marie Curie, Paris, France*

Received 12 November 2002; revised 6 May 2003; accepted 23 May 2003

Abstract

Large-scale runoff routing models (RRMs) are important as a validation tool for GCMs, and to close the hydrological cycle in fully-coupled climate models. The model RiTHM was developed to simulate the discharge of large rivers from the total runoff simulated by the LMD GCM. It uses a 1024×800 grid, nested in the 64×50 grid of the LMD GCM. The runoff simulated in a GCM grid cell is uniformly distributed over the underlying cells, where a series of two reservoirs accounts for the delay related to infiltration through the unsaturated zone and aquifers. The resulting riverflow is routed assuming pure translation along the drainage network, extracted with a GIS from a 5 min DEM. The transfer time from a cell to the outlet depends on topography, and on a basin-wide parameter, the time of concentration. RiTHM was calibrated in 11 river basins, using a realistic runoff forcing (computed by the land surface model SECHIBA from reanalyzed meteorological forcing). This led to a very satisfactory reproduction of observed hydrographs. The main problems were related to hydraulic processes neglected in RiTHM (reservoirs, diversion of riverflow because of flooding or irrigation). These results helped to validate SECHIBA, except for its snow processes, shown to be too simple. With the same parameters, RiTHM was also forced with runoff from the LMD GCM. This induced an important degradation of the simulated hydrographs, regarding both volume and timing. It was largely explained by errors in precipitation, and more generally climate, in the GCM. The direct calibration of RiTHM under the GCM-runoff forcing markedly improved the timing of simulated discharge, which could be interesting for land–atmosphere–ocean coupling. This work demonstrated that the usefulness of RRMs for GCMs strongly depends on their adequate calibration.

Keywords: River basins; Runoff routing; Discharge; GCMs; Land surface processes; Calibration

1. Introduction

The last decade has seen the development of many runoff routing schemes for general circulation models (GCMs). The main motivation behind this work is that

* Corresponding author. Address: UMR Sisyphe CNRS/UPMC, UPMC Boite 123, 4 place Jussieu, 75252, Paris cedex 05, France. Tel.: +33-1-44-27-51-27; fax: +33-1-44-27-51-25.
E-mail address: agnes.ducharne@ccr.jussieu.fr (A. Ducharne).

0022-1694/03/$ - see front matter © 2003 Elsevier B.V. All rights reserved.
doi:10.1016/S0022-1694(03)00230-0

runoff, as simulated by GCMs, is a local flux, given per unit surface. It is therefore fundamentally different from riverflow, which is needed for several purposes in the field of climate studies. Firstly, riverflow is very valuable for the validation of land–surface parameterizations. It integrates land-hydrology (and its response to land energy budgets) at large spatial scales, which are consistent with the GCM scale. Moreover, its measurements are numerous and highly accurate (Grabs et al., 1996).

Secondly, riverflow is required to close the global water cycling through oceans, atmosphere and land, and it should therefore not be neglected in coupled ocean/atmosphere GCMs. This fact is supported by many recent studies suggesting a wide spectrum of interactions between rivers and the climate system. An important consequence of fresh water input to the oceans is the creation of a barrier layer around some river mouths, which prevents the mixing of surface and deep waters and can thereby enhance local increases of sea surface temperature. This may influence convection, as shown by Murtuggudde (1998) in the tropical Atlantic, and by Weller (1998) in the Gulf of Bengal for the special case of the Indian summer monsoon. Mysak et al. (1990) suggest that variations of river discharge in the Arctic ocean alter its salinity and circulation, and therefore sea-ice transport through the Fram strait. In addition, Campos et al. (1999) suggest that discharge from the Rio de la Plata (Argentina) could be a link between ENSO (El Niño-Southern Oscillation) and the interannual variability of coastal currents along the Atlantic coast of South America (South Brazil Bight).

There are many different runoff routing models (RRMs) for large-scale river basins, and most of them, especially among those used in GCMs, belong to the 'linear-reservoir' RRMs. In such models, the grid-cells are linear reservoirs (characterized by a transfer coefficient, in time^{-1}), discharging into one another along the drainage network. A recent review can be found in Arora and Boer (1999). A common feature of most linear-reservoir RRMs is a rather coarse resolution, usually ranging from $5° \times 4°$ (mean cell area $\simeq$ 160,000 km^2; e.g. Liston et al., 1994; Miller et al., 1994) to $0.5° \times 0.5°$ (mean cell area $\simeq$ 2000 km^2; Vörösmarty et al., 1989; Hagemann and Dümenil, 1998). This may distort the influence of topography on transfer times, even though this problem can be corrected for sufficiently large basins (Fekete et al., 2001). The only higher resolution RRMs known to the authors are the models SWAM (Coe, 1998) and its descendant HYDRA (Coe, 2000), working at the $5' \times 5'$ resolution ($\simeq$ 10 km $\times$ 10 km at the equator).

This paper presents a new RRM, developed with special emphasis on high spatial resolution. This model, RiTHM (for River-Transfer Hydrological Model), is based on the hydrological model MODCOU (Ledoux, 1980; Ledoux et al., 1989). Both models are described in Section 2. Section 3 presents the design of this study, in which RiTHM was thoroughly assessed in 11 macro-scale river basins. An important point in this regard was to calibrate the parameters of RiTHM under a realistic runoff forcing, before using this model to transform runoff from a GCM into riverflow. Section 4 presents the results of these two stages, and of a complementary calibration under the GCM runoff forcing. Finally, in Section 5, the approach underlying RiTHM is summarized, and its limitations are discussed in the light of the above results.

2. Model description

2.1. The heritage: the hydrological model MODCOU

MODCOU (Ledoux, 1980; Ledoux et al., 1989) is a regional spatially-distributed model, which jointly describes surface and groundwater flow at a daily time step. At first, in every surface cell, surface runoff and deep infiltration are calculated from precipitation and potential evapotranspiration using a conceptual reservoir-based approach. Surface runoff is transferred through the drainage network with transfer times that depend on topography (length and slope of the downstream cells) and a basin-wide parameter, the time of concentration. Infiltration, on the other hand, recharges the groundwater (which can consist of multi-layered aquifers). A delay between surface infiltration and recharge to groundwater through the unsaturated zone can be included using a cascade of equal linear reservoirs (Nash, 1959). The recharge flow contributes to the dynamics of groundwater, given in each aquifer by a finite-difference solution of the two-dimensional diffusivity

equation. The resulting groundwater head is dynamically coupled to the water level in surface 'river' cells. Depending on the hydraulic gradient between the river and the groundwater, the latter contributes to riverflow or the river feeds the groundwater.

This model was successfully applied at different scales. French examples include, among others: the watersheds of the Haute-Lys (85 km^2) and the Caramy (250 km^2) (Ledoux, 1980); the watershed of the Fecht river (450 km^2) in the Vosges mountains (Ambroise et al., 1995); the HAPEX-MOBILHY study area of more than 14,500 km^2 in South-West France (Boukerma, 1987). MODCOU has also been tested in the French part of the Rhône basin, with a contributing area of 87,000 km^2 (Golaz, 1999; Habets et al., 1999). The last ongoing application of MODCOU (Gomez et al., 1999) involves the Seine river in the framework of the Piren-Seine research programme, devoted to the hydro-ecology of the Seine river basin ($\simeq$75,000 km^2). In this context, RiTHM can be seen as an adaptation of the hydrological model MODCOU to the macro-scale, for application to the largest river basins in the world.

2.2. RiTHM: overall framework

RiTHM was designed to be easily forced by total runoff simulated in the GCM of the Laboratoire de Météorologie Dynamique (LMD), by the land-surface scheme described in Section 3.1.1. Total runoff from any source, however, can be used as an input to RiTHM (see Section 3.1.3 for an example).

The main features of the LMD GCM are described in Sadourny and Laval (1984) and Le Treut and Li (1991). In this finite-difference, primitive equation model, the horizontal distribution of grid-points is regular in longitude and sine of latitude, defining grid-cells of equal area across the globe. The GCM runoff used in this study was computed using 64×50 grid-points in the horizontal, resulting in grid-cells of approximately 160,000 km^2 and a resolution in the tropics of about $5.6° \times 2.4°$.

As shown in the Niger basin (Fig. 1), the resolution of RiTHM is much finer than that of the GCM, since every GCM grid-cell is subdivided into 16×16 RiTHM cells. As in the GCM, the grid-points are distributed regularly in longitude and sine of latitude, and all the grid-cells in RiTHM have the same area of about 625 km^2. Total runoff (surface runoff + drainage from the soil) from a GCM cell is uniformly distributed over the 256 underlying RiTHM cells, where a 'riverflow production' module transforms runoff over the RiTHM cell into riverflow at the outlet of this RiTHM cell (Section 2.5).

Then, a riverflow routing module (detailed in Section 2.4) performs the downstream transfer of the riverflow from each RiTHM cell to the outlet of the river basin, at a daily time step. This routing is constrained by the drainage network, and Section 2.3 explains how it is extracted from a 5- min resolution digital elevation model (DEM), namely ETOPO5 (Edwards, 1989).

2.3. Drainage network characterization

Topography was interpolated to RiTHM's resolution from the 5- min resolution DEM ETOPO5 (Edwards, 1989). This resolution is consistent with the recommendations of Maidment (1996) to construct a global drainage network. The slopes dz/dx et dz/dy along the meridian and zonal directions were computed from the average elevation of each cell, using a third-order finite-difference method (Leblois and Sauquet, 2000; Cavazzi, 1995). The final slope was then given by

$$\tan \beta = \sqrt{(dz/dx)^2 + (dz/dy)^2} \quad (1)$$

and the flow direction by

$$\tan(\text{direction}) = \frac{dz/dx}{dz/dy} \quad (2)$$

In each cell, the latter was finally binned into one of four direction classes: north, east, south, and west. For example, the direction class 'east' comprises all directions in $]-\pi/4, \pi/4]$. This single-flow 4-direction network is inherited from the MODCOU model.

The resulting drainage network was not yet hydrologically sound. A classical problem is the existence of 'pits' (when the four possible neighbors of a cell have higher elevation, which interrupts the drainage network). A standard pit-removal algorithm (looking for a lower-elevation cell within a distance of three cells from the pit) allowed us to eliminate most

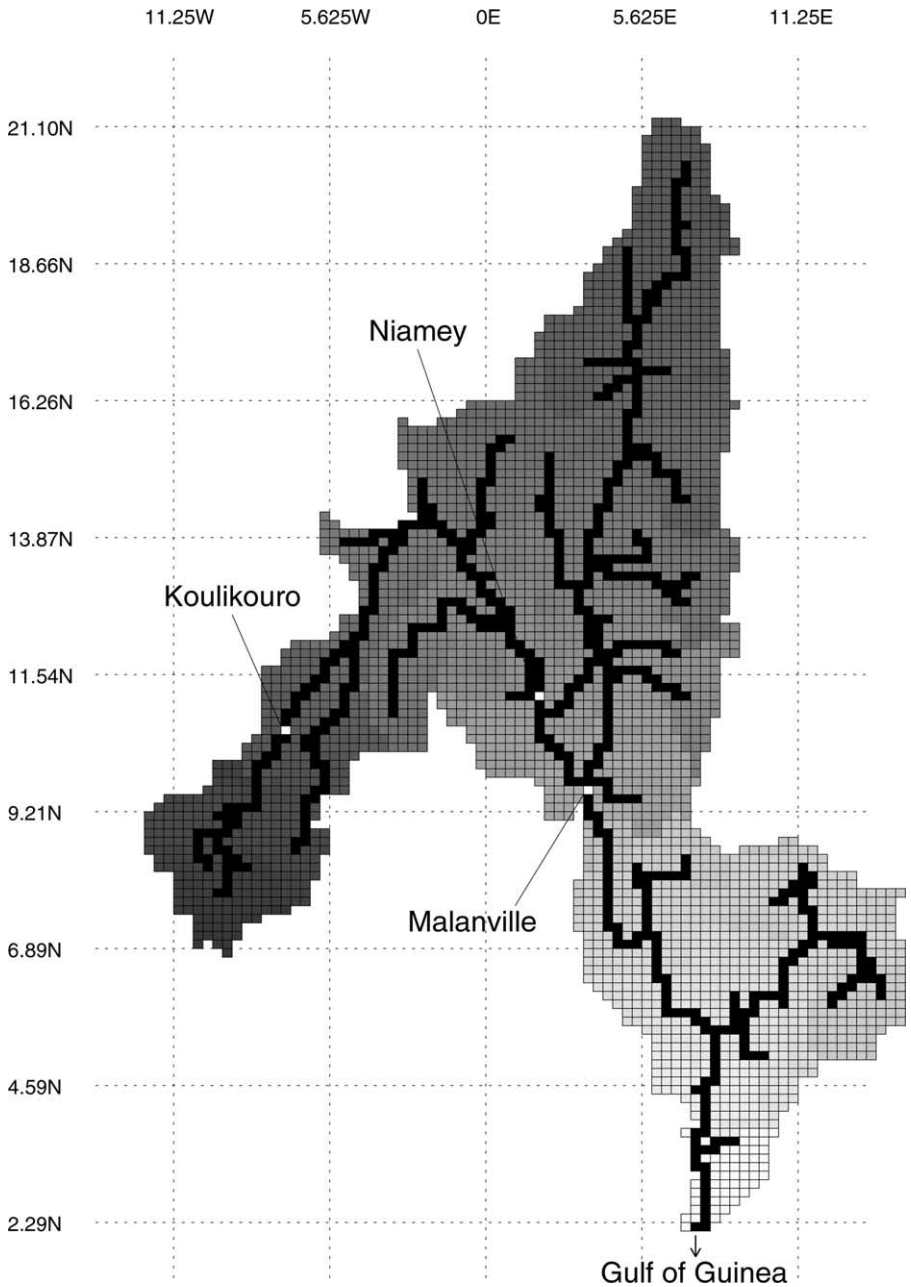

Fig. 1. Spatial coupling between RiTHM (fine grid) and the LMD GCM (coarse grid) in the case study of the Niger basin. In RiTHM's grid, the transfer times to the outlet (Section 2.4) decrease from dark to light gray, and the main river cells (contributing area larger than 150,000 km^2) appear in black. Three gauging stations are located: Koulikouro (Mali), Niamey and Malanville (Niger).

artificial pits, while ensuring that large natural depressions were retained.

Further corrections were needed to eliminate the remaining pits, and to assign a drainage direction in flat zones. Different methods have been proposed for these corrections. One of them is 'stream burning' (Maidment, 1996; Renssen and Knoop, 2000): the location of the main streams, derived

from maps or available datasets, is digitalized at the resolution of the drainage network, and this information is used to alter the mean elevation in the problem areas. We chose rather to perform corrections on flow directions, which were manually forced to mimic maps of the hydrographic network. Another problem was the artificial capture of one stream by another when the two streams happened in reality to flow in the same cell. This was also corrected manually, by forcing the two streams to flow in adjacent cells.

This 'manual' strategy is similar to the one used by Oki and Sud (1998). Where flow direction was modified, the original slope was kept, except of course in flat areas. There, a minimum slope $\tan\beta_0$ was imposed. We imposed a minimum elevation difference of 0.5 m between two connected cells in a flat area, leading to an average minimum slope $\overline{\tan\beta_0} = 2\times10^{-5}$ (i.e. 2 cm km^{-1}).

The corrected flow directions allowed us to recursively characterize the entire drainage network and delineate the boundaries of the river basins. Fig. 2 compares the resulting areas of 11 major river basins (shown in Fig. 6) to a reference value, which is the mean area of several published sources (Renssen and Knoop, 2000). It shows the excellent accuracy of the river basins areas in RiTHM. This figure also displays the areas estimated for each basin at the GCM resolution from a manual delineation (a GCM grid-cell being included either entirely or not at all in a river basin). There is a logical gain in accuracy when the resolution increases from the GCM to RiTHM, due to a better definition of basin boundaries. This effect contributes to improved basin-scale water budgets in RiTHM compared to the GCM.

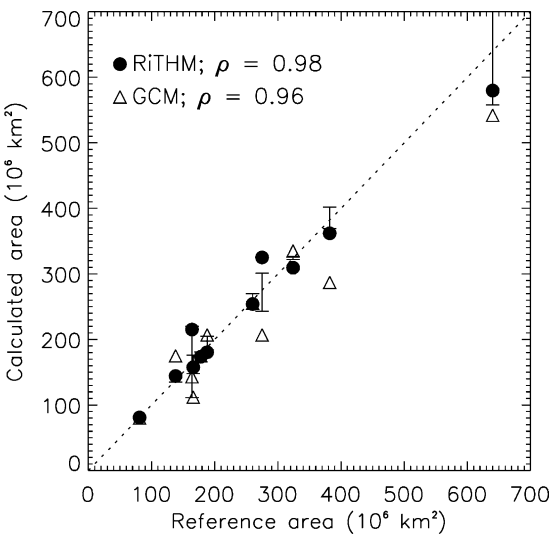

Fig. 2. Comparison of modeled area (at the resolution of RiTHM and the LMD GCM) and reference area, for the 11 large-scale river basins selected in this study (shown in Fig. 6). The reference area is the mean area of several published sources and the error bars indicate the minimum and maximum areas among these sources (Renssen and Knoop, 2000).

2.4. Riverflow routing

The main simplification of RiTHM compared to the hydrological model MODCOU is based on the assumption that, in any 625 km^2 grid-cell, there is at least one stream hydraulically connected to the water table. As a result, the water that infiltrates to the aquifer in a grid-cell—and is later transferred laterally in this aquifer—is drained by a stream in the same grid-cell where the initial infiltration took place. This assumes that the groundwater flow through a deep confined aquifer system is low in comparison to the flow through the phreatic one.

This assumption allowed us to discard the physical parameterizations related to groundwater: vertical infiltration through the unsaturated zone, groundwater flow and interactions between rivers and aquifers. In this simplified framework, the lag related to all these processes is created by only one infiltration reservoir, generating baseflow (Section 2.5). An important advantage of this simplification, beyond saving CPU, is to discard many parameters (thickness and vertical permeability of the unsaturated zone; structure, transmissivity, storage coefficient of aquifers; seepage coefficient describing head loss between river and aquifers). They are related to physical quantities that are not known in all studied river basins, and for which effective values at the grid scale are difficult to define.

Groundwater transfer being simplified into a baseflow component of riverflow, all water transfers across grid-cells occur in the surface drainage network, and we refer to this process as riverflow

routing. The latter is performed in RiTHM at a daily time step, under the assumption of pure translation. Thus, the transfer from one cell is completely independent from the transfer from any other cell, and from any possible interaction with the environment (as flooding, storage, evaporation, etc.). Under this assumption, the transfer time t_{adj} between two adjacent cells is defined by

$$t_{adj} = k \frac{d}{\sqrt{\tan \beta}} \quad (3)$$

where d is the distance and $\tan \beta$ the slope between the two grid-points, and where k is a scaling parameter, including the influence of roughness of the river bed. This formulation can be seen as a simplification of Mannings's formula (Dingman, 1994), the influence of the water stage being neglected.

At a larger scale, the river basin is characterized by two basin-wide quantities. L_{abs} is a purely topographical characteristic, equal to the sum of the ratio of distance to slope following the longest path (i.e. the path that maximizes the sum):

$$L_{abs} = \sum_{\text{longest path}} \frac{d}{\sqrt{\tan \beta}} \quad (4)$$

The time of concentration T_c is the only adjustable parameter of the routing module. It defines the time (in days) required to route water along the longest path, and allows us to scale coefficient k in Eq. (3):

$$k = T_c / L_{abs} \quad (5)$$

In this framework, k is uniform over the basin. This important simplification could be discarded. For example, one could separate k into the product of a roughness coefficient and a scaling coefficient depending on T_c. Note also that one application of MODCOU (Golaz, 1999) defines $k = k'/A_{sup}^{\alpha}$, where A_{sup} is the upstream contributing area, and α is positive, with values between 0.25 and 1. This formulation accounts for the increase of streamflow, thus of stream velocity, when the contributing area increases.

Because of its high resolution, RiTHM benefits from the efficient transfer algorithm of MODCOU, based on isochronous zones. For each cell, the transfer time to the outlet is the sum of the t_{adj} when one follows the drainage network from the chosen cell to the outlet. The basin is subdivided into isochronous zones, which comprise all cells having a transfer time to the outlet within the same day (in the present case of a daily time step). The corresponding total water volume is then transferred as a whole toward the outlet of the basin (or any predefined gauging station). Fig. 1 shows this framework for riverflow routing in the case of the Niger river basin. The transfer times to the outlet decrease from dark to light gray, when the distance to the outlet decreases, this effect being modulated by the influence of the slope. Such a method is equivalent to classical unit-hydrograph methods (Saghafian et al., 2002), but applied to a spatially distributed watershed, as in Olivera and Maidment (1999).

Fig. 3a shows the influence of T_c on the mean routed hydrograph at Malanville. This hydrograph was obtained by forcing RiTHM with the 10-year data set of runoff from the LMD GCM (Section 3.1.2). To illustrate the influence of T_c, we did not allow any infiltration in the riverflow module to delay riverflow compared to total runoff (see Section 2.5). Therefore, when $T_c = 0$, the hydrograph is equivalent to the spatial average of mean monthly total runoff over the contributing area at Malanville. The most direct influence of T_c is to lag the entire hydrograph, including peak discharge. The consequence is a dampened hydrograph, with slower floods and recessions. The effective lag between peak runoff and peak discharge is much shorter than the corresponding value of T_c : in the Niger basin, it is about 3 months for the 1-year T_c. Possible reasons are that (1) the hydrograph, measured at Malanville, does not correspond to the entire river basin, and (2) rainfall distribution is neither homogeneous nor constant throughout the basin.

2.5. Riverflow production

Riverflow production, which chronologically occurs before riverflow routing, is based on a two-reservoir conceptual model at a daily time step (Fig. 4). In every cell of RiTHM, the input runoff is first partitioned between surface runoff and infiltration, using a simple low-pass reservoir, of capacity C_s (in mm d^{-1}). At every daily time step, total runoff in excess of C_s is the surface runoff, which is

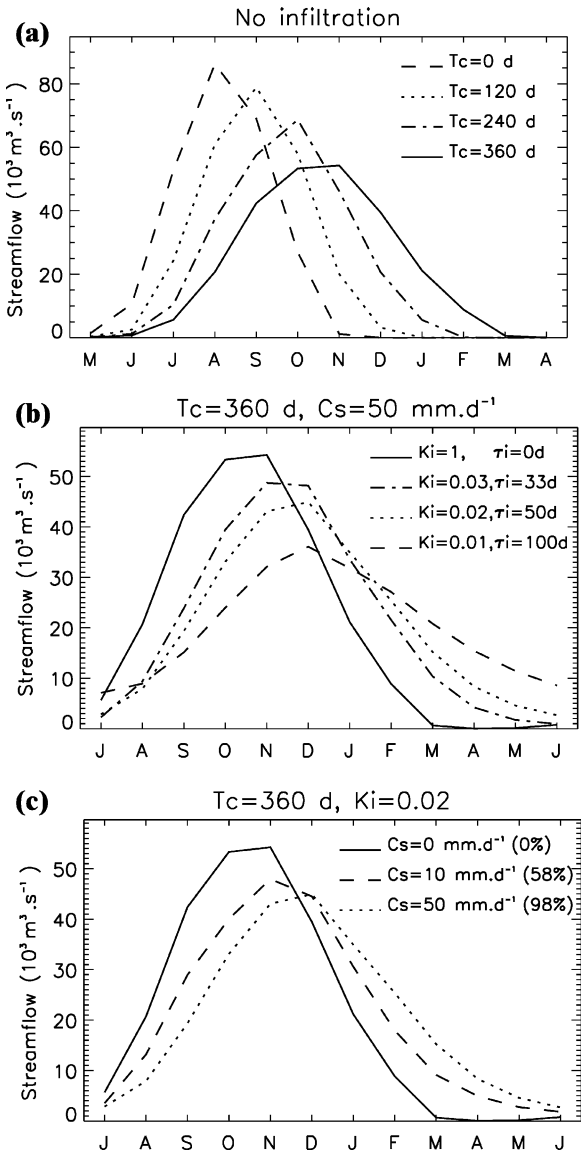

Fig. 3. Influence of the parameters of RiTHM on the simulated mean annual hydrograph, in the case of the Niger River at Malanville: (a) time of concentration T_c, with no infiltration allowed, (b) recession coefficient K_i (and residence time τ_i) and (c) capacity of the low-pass reservoir C_s, with $T_c = 360$ d. The time axis starts in May for (a) and in July for (b) and (c).

an instantaneous contribution to riverflow from the cell; the rest, lower or equal to C_s, is entirely transferred to an infiltration reservoir, through which it is delayed before being added to riverflow. Therefore, the latter is the sum of delayed baseflow and surface runoff.

The infiltration reservoir is characterized by a linear recession coefficient K_i (in d^{-1}), so that $Q_i = K_i S_i$ at each time step. In this equation, Q_i is the resulting delayed infiltration, also called baseflow in RiTHM, and S_i is the volume stored in the reservoir. This volume may be limited by a capacity C_i (in mm). However, to remove a non-linearity, this capacity was not used in this application.

Fig. 3 shows the influence of K_i and C_s on the mean annual hydrograph of the Niger river at Malanville (with $T_c = 360$ days). When $K_i = 1\ d^{-1}$, infiltration is not delayed by the infiltration reservoir and the only difference between total runoff from the GCM and streamflow is due to routing. The same behavior occurs when $C_s = 0$ mm d^{-1}, which cancels infiltration.

The parameter K_i controls the storage in the infiltration reservoir. It is related to the residence time τ_i (d) in this reservoir, which is defined as the time required to divide any stored volume by e ($\simeq 2.718$), and corresponds to the time lag between the centroids of runoff and riverflow from the cell (Dingman, 1994). When K_i decreases (Fig. 3b), the residence time increases, leading to slower floods and recessions. It results in a flatter hydrograph and a delayed peak discharge. A similar lagging and dampening of the hydrograph happens when C_s increases (Fig. 3c), because more water is then delayed by infiltration.

The values examined here for K_i (0.01, 0.02, 0.03 d^{-1}) are the ones allowed in RiTHM. They correspond to residence times τ_i between 100 and 33 d, in the range of published values (Pilgrim and Cordery, 1992; Liston et al., 1994; Hagemann and Dümenil, 1998; Arora and Boer, 1999) for interflow (return flow from infiltration in the unsaturated zone) and baseflow (return flow from groundwater). They tend to be smaller than the K_i values commonly used in MODCOU, that range between 0.1 and 0.02 d^{-1} (Ledoux, 1980; Gille, 1985; Boukerma, 1987). The reason is that the infiltration reservoir of RiTHM accounts for the delay caused not only by infiltration into the soil, but also by vertical flow through the unsaturated zone and by the much slower horizontal groundwater flow, both explicitly described in MODCOU.

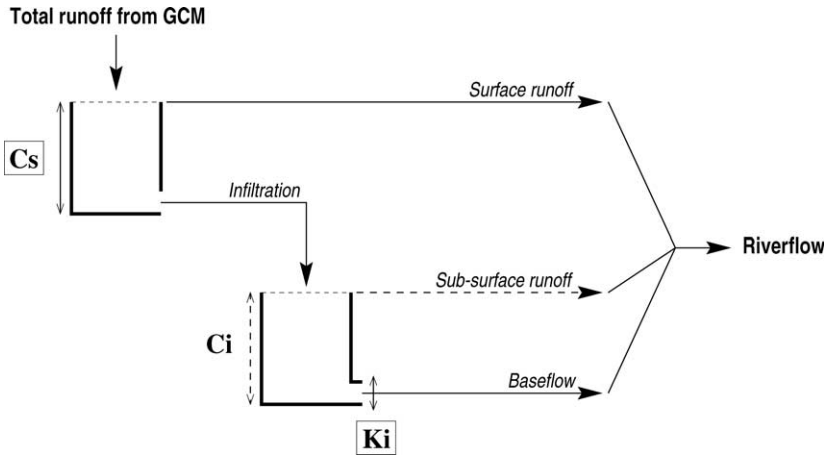

Fig. 4. Illustration of the transformation of total runoff from the GCM into riverflow, through a series of two reservoirs characterized by three parameters C_s, K_i and C_i (the latter is optional).

3. Design of the study

3.1. Runoff input

3.1.1. The land surface model SECHIBA

Runoff in the LMD GCM is calculated at a 30 minute time step by the land surface model (LSM) SECHIBA (Ducoudré et al., 1993). This model represents vegetation owing to the 'mosaic' strategy (Avissar and Pielke, 1989; Koster and Suarez, 1992): the heterogeneous vegetation cover of a GCM grid-cell is described by a set of homogeneous 'tiles', each tile representing a different land surface type (bare soil or one of seven vegetation types). The total evaporation is computed as the weighted average of the contributions from all the tiles in a grid-cell. The modeled evaporative fluxes from each tile are: interception loss (evaporation of the water intercepted by the canopy), snow sublimation, bare soil evaporation and transpiration, controlled by resistances increasing with environmental stresses (dry soil, dry air, high insolation).

Water can be stored in the canopy interception reservoir, a one-layer snow pack and a two-layer soil reservoir. The original functioning of the latter is based on Choisnel's ideas (Ducoudré et al., 1993; Choisnel et al., 1995) and described in detail in Ducharne and Laval (2000). The depth of active soil is one meter and the water-holding capacity is globally equal to 150 kg m^{-2} (except in deserts where it is set at 30 kg m^{-2}). The described soil hydrological processes are (i) the partitioning between surface runoff and infiltration into the soil, (ii) the diffusion between the two soil layers, and (iii) drainage from the soil. The parameterization of surface runoff relies on a statistical–dynamical description of the small-scale variability of soil, known as the Arno (Dümenil and Todini, 1992; Rowntree and Lean, 1994) or VIC (Wood et al., 1992; Liang et al., 1994) approach. It introduces a subgrid-scale distribution of local storage capacity, with local capacities smaller than 150 kg m^{-2} that can reach saturation and give rise to runoff before the saturation of the whole grid-cell.

The snow processes, and their influence on runoff, are very simple in SECHIBA. The one-layer snow pack is represented by one water-equivalent prognostic variable, expressed in mm of water. This term is increased by snow fall (the form of precipitation when air temperature is below freezing) and decreased by snow sublimation and snow melt (all three terms in mm of water). Snow melt occurs when the surface temperature of a cell is above freezing, at the rate which insures that the surface temperature (here the snow temperature) does not exceed 273.15 K. The resulting water flux comprises, together with throughfall, the water that is partitioned between surface runoff and infiltration. The corresponding energy flux is considered in the surface energy budget and influences the surface temperature of the cell.

3.1.2. Runoff simulated on-line in the LMD GCM

In this study, we used runoff from a 64×50 resolution simulation of the LMD GCM, coupled to the above version of the LSM SECHIBA. In this simulation (Ducharne et al., 1998; simulation 'TOT'), the LMD GCM was forced with 10 years (1979–1988) of interannually varying sea surface temperatures (SST) from the AMIP dataset (Gates, 1992). Note that, for all RiTHM simulations forced with the above GCM runoff, only the last 9 years of streamflow were considered, as the first T_c days of the simulation are incorrect by lack of sufficiently anterior runoff. This also allows the infiltration reservoir to spin-up.

Compared to available climatologies, the above GCM simulation shows a large overestimation of mean precipitation over land ($P_c = 1021$ mmy^{-1}). For instance, Legates and Willmott (1990) provide an estimate of 820 mm y^{-1} for gauge-corrected precipitation over land. Such overestimation of mean precipitation over land (large enough to be significant despite disparities in the time period of the simulation and the climatologies) is related to a systematic overestimation of total runoff ($R = 503$ mm y^{-1}) and continental evaporation ($E_c = 518$ mmy^{-1}), yet to a smaller extent. The marked overestimation of total runoff is associated with excessive moisture convergence over land (approximated by $P_c - E_c$ as the interannual variations of soil moisture can be ignored), itself related to excessive moisture divergence over the oceans by means of water balance.

Beyond global water budgets, Fig. 5 shows the main weaknesses of the simulation used in this study in terms of spatial patterns. The overestimation of precipitation is especially strong over mountainous areas (where it is persistent most of the year) and in the Inter-Tropical Convergence Zone. The regional underestimations of precipitation are usually weaker, and one reason is that they are seasonal to a large extent. This is the case in Amazon basin, where the main underestimation of precipitation happens during the rainy season. This is also the case in the northern hemisphere rainbelts (Europe and eastern North-America), where it is underestimated in summer, while overestimated in winter, although to a lesser extent. A more detailed analysis of this simulation can be found in Ducharne et al. (1998).

3.1.3. Runoff simulated off-line from ISLSCP meteorological forcing

Because of the important bias in precipitation and runoff in the above GCM simulation, we used another runoff data set, supposedly more realistic, to evaluate the performances of RiTHM.

This runoff comes from a two-year stand-alone simulation of the LSM SECHIBA, performed at the $1° \times 1°$ resolution. We called it the ISLSCP runoff since all of the required atmospheric and boundary

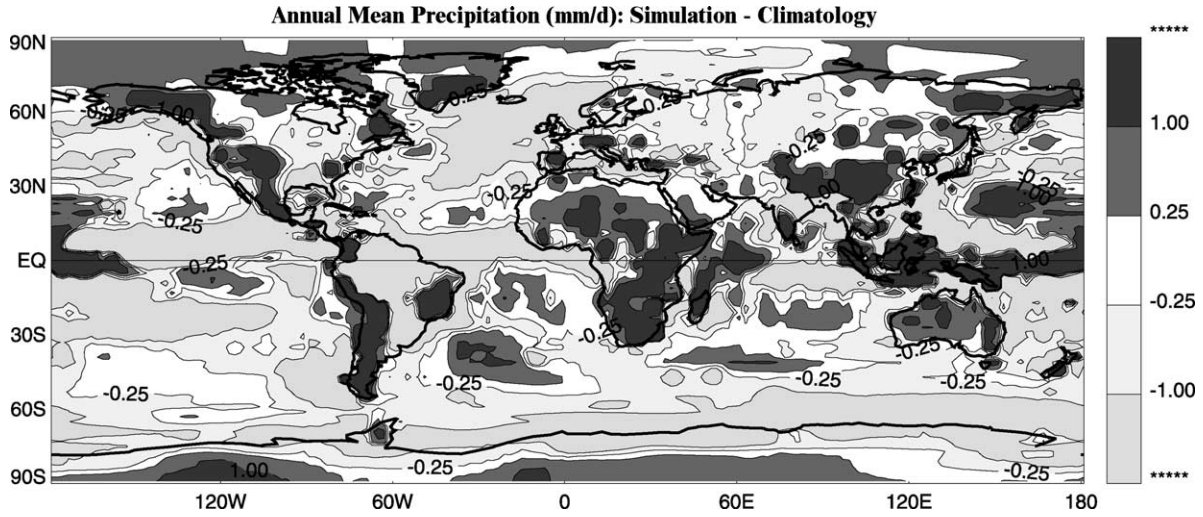

Fig. 5. Precipitation difference (in mm d^{-1}) between the mean annual field simulated by the LMD GCM over 1980–1988 and the annual climatology of Legates and Willmott (1990).

conditions data sets were given by the ISLSCP Initiative I data set for 1987–1988 (Sellers et al., 1996), at the $1° \times 1°$ resolution across the globe. Global fields of precipitation, incoming long-wave and short-wave radiation at the surface, and near-surface temperature, humidity, pressure and wind speed, have various observational sources. They are processed with a data assimilation system in order to extrapolate them spatially across the globe and to interpolate them to a 6 h timescale. The general framework for the off-line integration of SECHIBA with the ISLSCP Initiative I data set for 1987–1988 was based on the recommendations of the Global Soil Wetness Project (Dirmeyer and Dolman, 1998). In particular, to avoid non-equilibrated spin-up signal, the forcing corresponding to 1987 had been repeated until the model had reached equilibrium.

As an input to RiTHM, we used runoff from the last 3 years of this integration (the last 2 years corresponding to 1987 and the year corresponding to 1988), then we discarded the first year of simulated streamflow. This allowed us to analyze two full years of simulated streamflow. The first T_c days in this streamflow time series, however, are erroneous, since they were computed from an atmospheric forcing from 1987 instead of 1986. Furthermore, runoff from 1987 (and therefore streamflow until the T_cth day of 1988) might be altered by the equilibrium of 1987 soil moisture with 1987 atmospheric conditions, which is required to get sensible initial conditions, but does not guarantee realistic initial conditions.

To limit questions regarding resolution when comparing results from RiTHM forced with the GCM runoff and with the above off-line runoff, we chose to alter the resolution of the latter, and upscale it to the GCM resolution. Therefore, RiTHM could be forced with this off-line runoff without undergoing any modification. Also, there was one difference in SECHIBA compared to the version used in the GCM, as the so-called Arno parameterization for surface runoff was not implemented. The upscaling of the resulting off-line runoff overrode to some extent this difference.

3.1.4. Why use total runoff as an input to RiTHM?

We showed how the riverflow production module (Section 2.5) uses a low-pass reservoir of capacity C_s to partition the input total runoff into surface runoff and infiltration, the latter being delayed through an infiltration reservoir to form baseflow. It could also be possible to bypass the low-pass reservoir and use the partitioning between surface runoff and infiltration realized by SECHIBA (SECHIBA's drainage corresponds to RiTHM's infiltration). This partitioning, however, is among the 'weak links' in most LSMs (Koster et al., 2000), and it may become very unreliable when LSMs are coupled to GCMs, because of the systematic errors in GCM precipitation (as shown with the LMD GCM in Section 3.1.2).

3.2. Application to 11 macro-scale river basins

The required drainage network was characterized for 152 of the largest river basins around the world. They cover a high fraction of land masses, with the exception of smaller coastal river basins and endorheic basins. Eleven of the largest river basins, shown in Fig. 6, were selected to test RiTHM, based on the availability of observed streamflow data and the representativity of the hydrometeorology of these basins.

Our primary goal was to evaluate the skills of the association of RiTHM and the GCM to reproduce observed streamflow, with a focus on climate studies. An important concern, however, was the strong systematic errors of the LMD GCM on precipitation and total runoff (Section 3.1). This prevented the time-accumulated volume of streamflow from being accurate, and hindered any good calibration of simulated streamflow to the observed one. More importantly, it prevented us from assessing the individual performances of RiTHM, and its contribution to the overall error. We addressed this part of the problem by using a more realistic runoff input to RiTHM, namely the ISLSCP runoff, simulated off-line by SECHIBA under the ISLSCP forcing.

3.3. Validation data

3.3.1. RiTHM forced with GCM runoff

For comparison with the streamflow simulated from the GCM runoff, we considered observed streamflow data from two often redundant sources: the Global Runoff Data Center (GRDC, Koblenz, Germany) and the ISLSCP Initiative I data set. These data themselves originate for a large part from UN

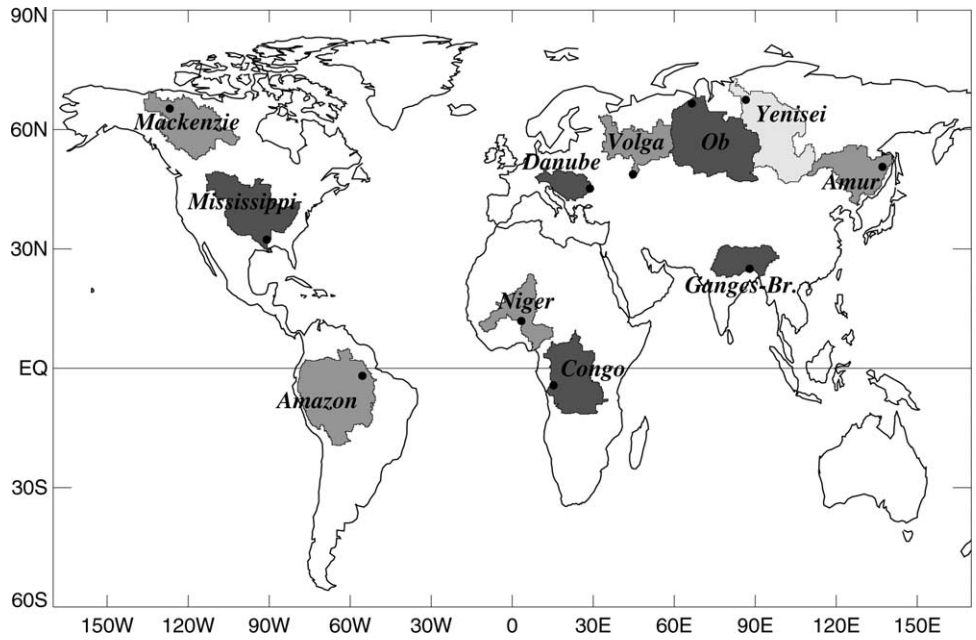

Fig. 6. Location of the 11 selected river basins and their downstream gauging stations (dark dots).

Educational, Scientific and Cultural Organization data (UNESCO, 1993). In each basin, we selected the furthest downstream available gauging station (Fig. 6), where streamflow integrates runoff from a large fraction of the basin. Additional gauging stations can be considered, of course, as illustrated in the case of the Niger river (Fig. 1).

Most observed streamflow data were given monthly, with gaps in the time series, and over a time frame that generally had, at best, a few years in common with the 1979–1988 GCM simulation period. Therefore, simulated and observed streamflow were compared in each basin in terms of their inter-annual mean hydrograph (composed of 12 mean monthly values of discharge). They were constructed over 1980–1988 for the simulated discharge, and over the entire available period for the observed discharge (climatological means). Similarly, monthly mean precipitation rates simulated in the LMD GCM on average over 1980–1988 were compared, over each river basin, to the gauge-corrected monthly climatology of Legates and Willmott (1990).

3.3.2. RiTHM forced with ISLSCP runoff

Complementary data were needed to evaluate the streamflow simulated by RiTHM from the off-line runoff based on the ISLSCP forcing, because the 1987–1988 period was very poorly represented in the above sources of measured streamflow. In the framework of the Global Soil Wetness Project, monthly river discharge from 1987–1988 was collected from 250 stations in 150 river basins (Oki et al., 1999), including ten of the 11 selected basins (Amazon, Yenisei, Mississippi, Ob, Ganges, Amur, Volga, Danube, Niger, Mackenzie). For the Congo river, monthly discharge data from 1987–1988 were found in the RivDis database (Vörösmarty, 1996), at the Brazzaville gauging station.

4. Results

4.1. Calibration of RiTHM under the ISLSCP runoff forcing

4.1.1. Preliminary analysis

The annual mean discharge simulated by RiTHM forced with the ISLSCP runoff is very realistic compared to observations (Fig. 7) in 10 of the 11 selected river basins (the mismatch in the Niger basin will be discussed in Section 4.1.2). This result validates the ability of SECHIBA to correctly

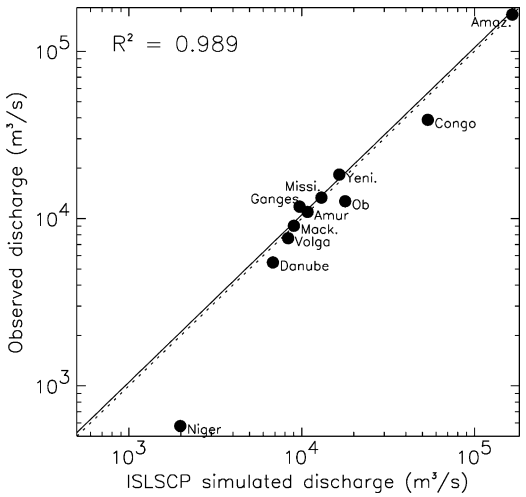

Fig. 7. Comparison of mean annual streamflow, simulated by RiTHM forced with the ISLSCP runoff, vs. observed in 1987–1988, in the 11 selected river basins. The dotted line is the 1:1 line, and the solid line corresponds to the log-log regression.

partition precipitation between evaporation and runoff at the annual time scale. Thus, it justifies the use of this runoff forcing to calibrate the free parameters of RiTHM, namely T_c, C_s, and K_i, so that observed streamflow was correctly reproduced in these 11 river basins. In each of them, observed discharge was provided in one downstream station, as 24 monthly values, and this prevented us from detailed calibration. In particular, even though C_s and K_i are distributed parameters, we chose to keep them uniform in each river basin, because of insufficient information. We also performed the calibration manually, and tried to reproduce firstly the timing of floods and recessions, then, if possible, the general shape of the hydrograph.

4.1.2. Calibrated hydrographs

Fig. 8 shows the result of this calibration exercise. In agreement with Fig. 7, the magnitude of streamflow is good, except in the Niger and Congo basins, and to a lesser extent in the Danube basin. The figure also shows that the relative magnitude of high and low flows is correctly simulated. This results from the ability of SECHIBA to transform the atmospheric forcing into runoff at the monthly time scale, but also from the storage allowed by RiTHM. In some basins, however, corresponding to rivers influenced by large reservoirs (either natural as on the Yenisei or Mackenzie, or artificial as on the Volga or Mississippi), the low flows are systematically underestimated, because the reservoirs and their storage cannot be accounted for in RiTHM. Finally, the timing of floods and recessions in the simulated hydrograph, related to the lag introduced in RiTHM by the time of concentration T_c and the storage (C_s and K_i), agree well with observations.

Many objective criteria exist to assess the quality of riverflow simulations compared to observations. The linear correlation coefficient is among the simplest ones. It measures the covariance of the simulated and observed time series, and therefore tells if the variations in simulated streamflow (floods, recessions) have a realistic timing. The efficiency of Nash and Sutcliffe (1970) also derives from linear regression techniques, but includes information about the departures between the simulation and the observation. It varies from $-\infty$ to 1. The optimal value is 1 (perfect agreement between observed and simulated time series), and values greater than 0.7 are usually accepted as satisfactory.

In many basins, simulated streamflow agrees better with observations in 1988 than in 1987 (e.g. Ob, Volga), and the most poorly simulated months are the first ones in 1987 (e.g. Mississippi, Danube). It is likely the result of a poor initialization of soil moisture (discussed in Section 3.1.3). Therefore, the two above criteria (Table 1) were computed only for 1988. They confirm that the calibration was satisfactory. Four basins have efficiencies lower than 0.7; their correlation coefficient, however, is always significant and greater than 0.7, which shows that the general shape of the hydrograph is well represented by the model. However, some problems remained: enhanced hydrological contrasts (Mississippi, Volga), underestimated spring flood in the Amur, overestimated winter flood in the Danube. Except for the neglected effect of reservoirs, these problems are most likely related to the simulation of runoff by SECHIBA. Given the location of these basins, we strongly suspect problems related to snow processes, which are very simplistic in SECHIBA (Section 3.1.1).

In the Congo and the Niger basins, the efficiency is negative, because of the systematic overestimation of simulated streamflow displayed in Fig. 8. In the Niger basin, the main reason for this overestimation is that RiTHM does not account for

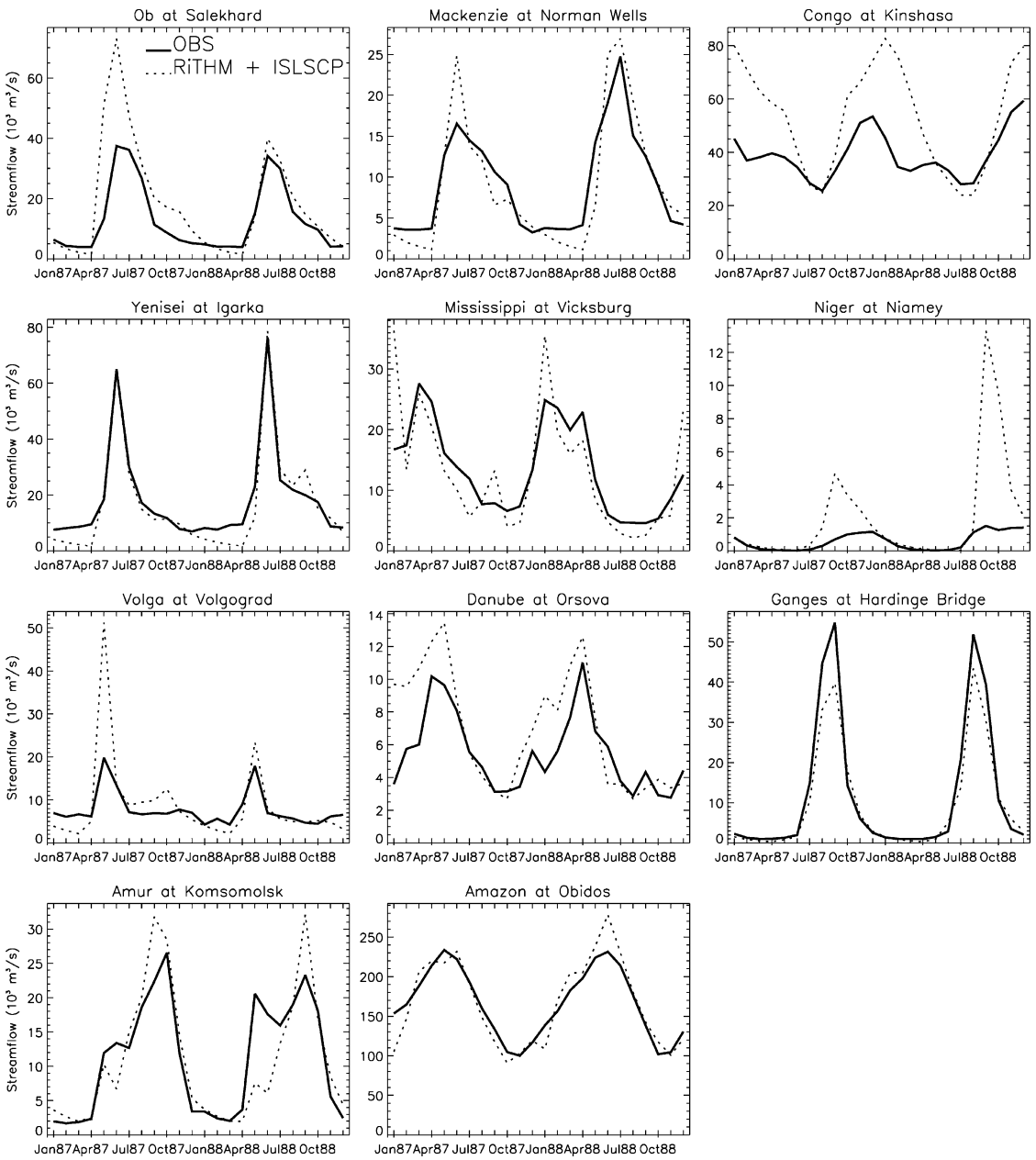

Fig. 8. Monthly streamflow simulated in 1987–1988 by RiTHM forced with the ISLSCP runoff: comparison with 1987–1988 observed discharge in the 11 selected river basins. See text for further explanations.

the diversion of riverflow through the inner delta of the Niger (related to flooding and irrigation). The latter is clearly shown by the decrease of observed annual mean streamflow along the delta (Fig. 1), from Koulikouro (1407 m^3/s for a contributing area of 120,000 km^2) to Niamey (893 m^3/s for 700,000 km^2) to Malanville (1053 m^3/s for 1,000,000 km^2). The overestimation of simulated streamflow downstream in the Congo is likely related to similar reasons (i.e. the diversion of

Table 1
Results of the calibration of RiTHM forced with the ISLSCP runoff in the selected 11 river basins: calibrated parameters (T_c is related to a mean velocity U, C_s to the percentage of total runoff that infiltrates over the simulation period, and K_i to the residence time τ_i), and criteria quantifying the quality of the simulations. The latter are the efficiency of Nash and the Spearman's rank-order correlation coefficient ρ between the 12 monthly values of simulated and observed discharge in 1988

Rivers	T_c (days)	U (m^{-1})	C_s (mm d^{-1})	C_s (%)	K_i (d^{-1})	τ_i (days)	Nash (−)	ρ (−)
Ob	90	0.96	7	25	0.02	50	0.91	0.93*
Yenisei	120	1.39	1.3	50	0.01	100	0.90	0.77*
Volga	45	0.76	3	66	0.01	100	0.55	0.70*
Amur	90	0.40	1.05	50	0.01	100	0.49	0.82*
Mackenzie	165	0.42	2	66	0.01	100	0.75	0.93*
Mississippi	45	0.75	1	50	0.01	100	0.57	0.94*
Danube	105	0.48	0.4	25	0.02	50	0.23	0.72*
Amazon	240	0.22	3.5	50	0.02	50	0.79	0.94*
Congo	360	0.14	4	66	0.01	100	−3.55	0.70*
Niger (Niamey)	135	0.38	2.9	50	0.02	50	−50.14	0.88*
Ganges-Br.	75	0.43	1.5	10	0.02	50	0.93	0.99*

*/† indicates a significant correlation at the level $\alpha = 0.05/0.10$.

riverflow through the extensive floodplains along the river, which is not simulated by RiTHM). The scarcity of streamflow observations along its main course, however, prevents any firm conclusions.

4.1.3. Calibrated parameters

The parameters resulting from the above calibration are given in Table 1. The time of concentration T_c can be related to a mean velocity U over the basin. With the exception of the Yenisei, it falls in the range 0.15–1.00 m s^{-1} used by many authors for large-scale river velocities (see review by Oki et al. 1999). The values used for C_s are in the range of the hydraulic conductivity of soils (Rawls et al., 1992). It is also interesting to relate this parameter to the percentage of total runoff that infiltrates in a given basin over the simulation period. The highest values may be overestimated because the infiltration reservoir in RiTHM compensates for the lack of storage in neglected hydraulic annexes, as lakes and reservoirs (see the Volga and Mackenzie with C_s yielding to 66% of infiltration) or floodplains (Congo, Amazon).

Since the calibration was manual, it is likely that we did not try all the combinations of parameters that could give similar (or even better) results than the combination selected in Table 1, in terms of subjective adjustment and quantitative criteria. In any case, we did not try to optimize these criteria, and we deliberately chose to preserve some likelihood to the calibrated parameters. We preferred infiltration percentages lower than 50%, unless there were good reasons to use higher values (as well-known reservoirs or floodplains, which create important lag). Even in these cases, we did not accept infiltration percentages higher than 66%, which would have been a trade-off for neglected processes. Similarly, we did not consider $K_i = 0.005$, corresponding to a residence time $\tau_i = 460$ d in the infiltration reservoir.

4.2. RiTHM forced with GCM runoff

4.2.1. Parameters from the above calibration

As an attempt to evaluate runoff from the LMD GCM, we used it to force RiTHM, with the parameters calibrated above using the more realistic ISLSCP runoff (Table 1). One must keep in mind, however, that the infiltration percentage corresponding to a given value of C_s varies with the features (mean value, short-term dynamics) of the runoff forcing. Since they can differ markedly between the ISLSCP and GCM runoff, we kept the infiltration percentages from Table 1 rather than C_s, in order to maximize the similarities between the simulations.

The comparison of Figs. 8 and 9 shows a clear deterioration of the simulated hydrographs when the GCM runoff forcing is used. Total volume is the most poorly reproduced feature of the simulated discharge. This problem is very general (with the only exception of the Amur) and explains most of the decrease in Nash's efficiency (Table 2 compared to Table 1).

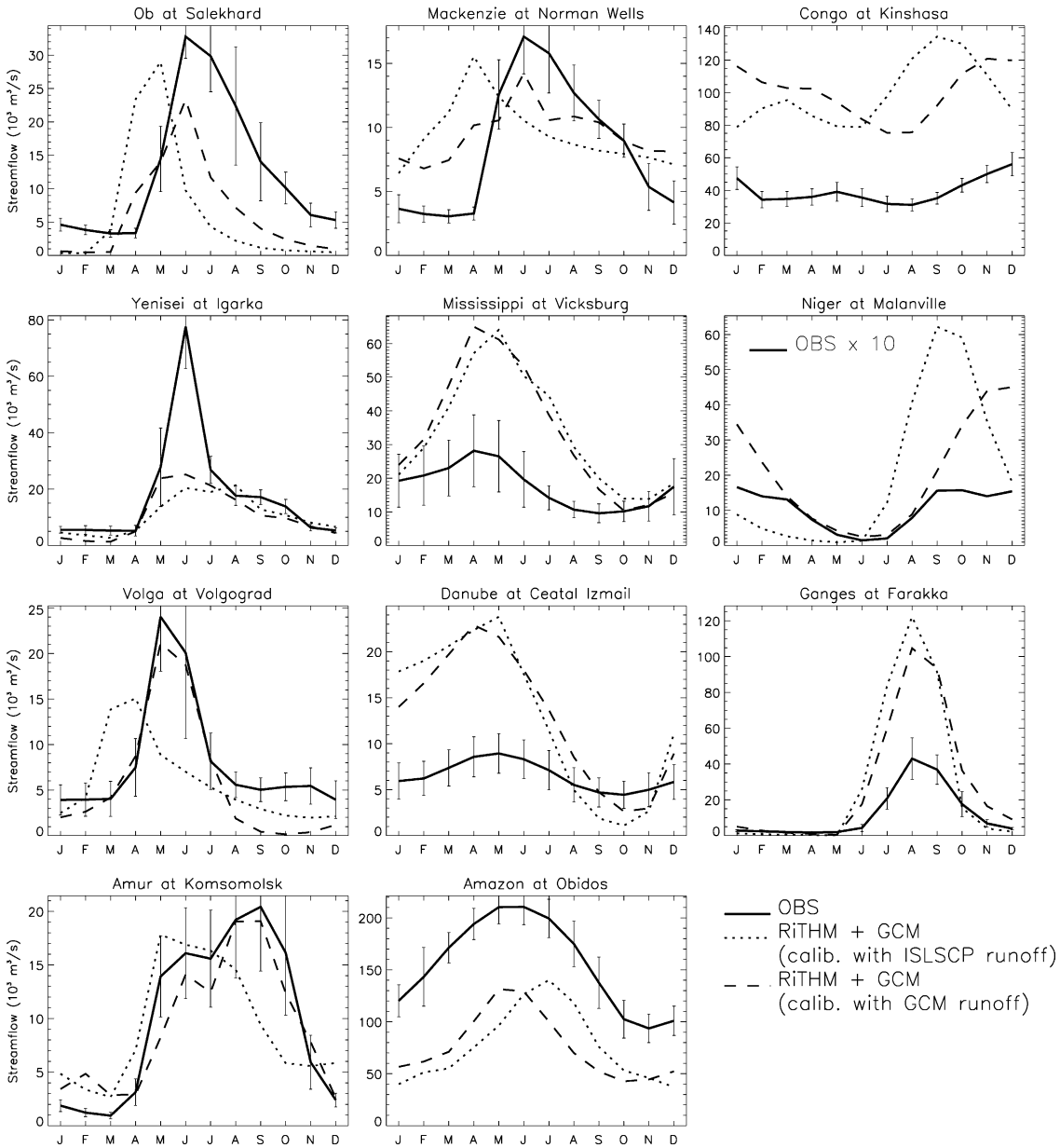

Fig. 9. Mean annual cycle of streamflow in the 11 selected river basins: results from RiTHM forced with GCM runoff according to two different calibrations (calibration based on ISLSCP runoff in dotted lines; direct calibration from GCM runoff in dashed lines), compared to climatological streamflow (see Section 3.3.1). The vertical bars define the standard deviation of monthly observed streamflow over the record period (except for the Niger at Malanville).

Many hydrographs simulated from the GCM runoff also display flaws in the timing of floods, which induce a decrease in the correlation coefficients between the simulated and observed hydrographs (Table 2).

This increase in the departures from observed discharge values is largely related to differences between observed and GCM-simulated climate. Firstly, the departure in volume is directly tied to the bias in annual discharge (Table 2). The latter is

Table 2
Summary of the results of RiTHM run with GCM runoff and parameters calibrated using ISLSCP runoff: comparison of observed (OBS) and simulated (RiTHM) streamflow, and related bias, Nash's efficiency and Spearman's rank-order correlation coefficient ρ; comparison of observed (OBS) and simulated (GCM) prcipitation, and related bias

Rivers	Streamflow (10^3 m^3 s^{-1})					Precipitation (mm y^{-1})		
	OBS	RiTHM	Bias	Nash	ρ	OBS	GCM	Bias
Ob	12.5	6.3	−6.2	−1.08	0.37	513	367	−146
Yenisei	17.8	10.7	−7.1	0.23	0.87*	423	476	53
Volga	8.1	5.8	−2.3	−0.20	0.50	659	508	−151
Amur	9.7	9.2	−0.5	0.53	0.68*	576	671	95
Mackenzie	8.4	9.5	1.1	−0.26	0.06	361	632	271
Mississippi	17.6	33.6	16.0	−10.05	0.71*	865	960	95
Danube	6.5	12.9	6.4	−39.09	0.92*	884	1072	188
Amazon	154.9	76.3	−78.6	−2.82	0.84*	2205	1413	−792
Congo	39.5	99.4	59.9	−69.09	−0.30	1606	1955	349
Niger (Malanville)	1.1	20.6	19.2	−2754.	0.63*	797	1166	369
Ganges-Br	12.0	29.0	17.0	−4.91	0.97*	1436	2049	613

*/† indicates a significant correlation at the level $\alpha = 0.05/0.10$ between the 12 monthly means.

very high (compared to observed annual discharge for instance), which agrees with the above observations. Furthermore, its sign is generally identical to the sign of the bias in precipitation. The clearest examples of the propagation of systematic error from precipitation to simulated discharge is found in the Ganges and Amazon (Fig. 10). In the rest of this section, we will focus on selected cases, to illustrate more complex sources of error in the discharge simulated by RiTHM forced with the LMD GCM runoff.

High-latitude rivers are strongly impacted by snow; floods occurs in spring, before the precipitation maximum, and are therefore due to snowmelt. In the Ob, Yenisei, Volga and Amur, the spring floods simulated by RiTHM tend to be too weak and too early. This problem in both volume and timing might be related to possible weaknesses of SECHIBA regarding surface snow processes, as mentioned in Section 4.1.2. It is also consistent with the LMD GCM overestimating 2- m air temperature by several degrees at high latitudes (compared to the climatology of Legates and Willmott (1990) based on the 1950–1996 period; not shown), which can decrease snowfall and advance snowmelt.

Another common feature between the above four rivers is that the LMD GCM markedly underestimates summer precipitation. This enhances the underestimation of simulated streamflow during the recession period in the Ob, Yenisei and Volga basins, and in the Amur, the second flood is completely missed by the simulation because it is related to rainfall rather than snowmelt. These lows in summer GCM precipitation also explain the strong negative biases in annual precipitation in the Ob and Volga (Table 2). In the Yenisei and Amur, GCM precipitation also exhibits a strong overestimation in winter and spring, when precipitation is not directly available for runoff because of snow processes. This explains why these two rivers experience opposite biases in precipitation and streamflow. The Danube and Mississippi basins also show an underestimation of summer rainfall, but it is combined to an overestimation of winter precipitation. There, the latter exceeds the former, and snow and snowmelt are less important than in the higher latitude rivers; therefore, the simulated discharge is overestimated, like precipitation.

Another type of relationship between the errors in GCM precipitation and those in simulated discharge is illustrated by the case of the Congo (Fig. 9). Simulated discharge has an opposite phasing to the observed discharge (as also shown by the negative correlation coefficient in Table 2. However, RiTHM and its parameters do correctly capture the phase of the Congo hydrograph with a realistic precipitation forcing (Fig. 8), and the mean annual cycle of precipitation is correctly captured by the GCM, even if the annual mean is too high (Fig. 10). Therefore,

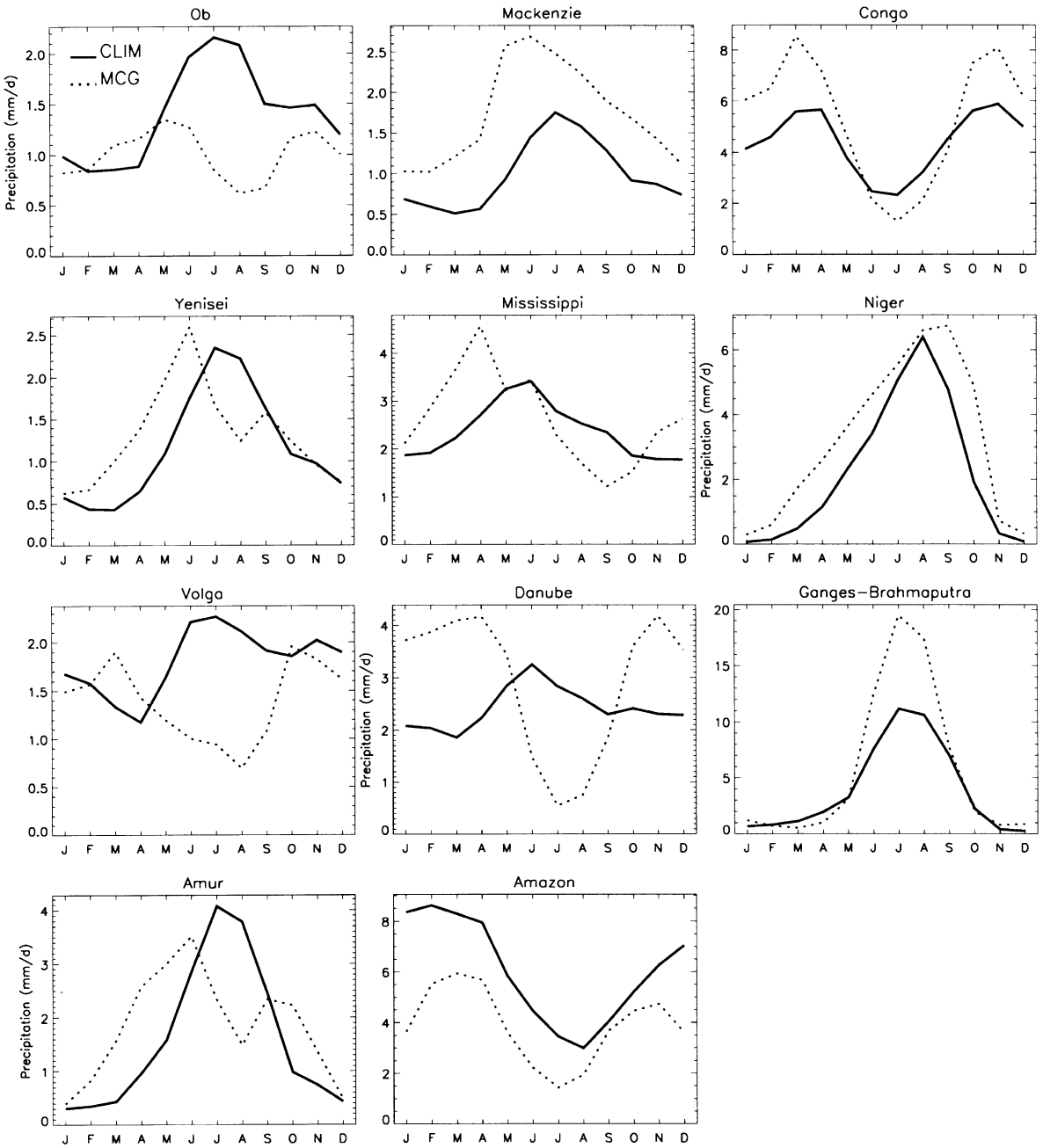

Fig. 10. Mean annual cycle of simulated and climatological precipitation (regional averages over the 11 selected basins). The precipitation climatology is from Legates and Willmott (1990).

the most likely explanation of the phasing error is an incorrect spatial distribution of rainfall over the Congo basin by the GCM, which shifts the location of maximum rainfall from the center of the basin to the the reliefs on its borders (Ducharne, 1997), as a result of enhanced topographical precipitation (Section 3.1.2). Problems with the spatial patterns of GCM precipitation also explain the poor timing

of simulated discharge in the Mackenzie river (Ducharne, 1997).

4.2.2. Parameters from direct calibration with GCM runoff

Not surprisingly, the previous section has shown that errors in the runoff forcing propagate into the simulated streamflow and lead to unrealistic hydrographs. This is true even with a realistic RRM, such as RiTHM when it is calibrated with the ISLSCP runoff forcing. For climate studies, however, especially regarding land–atmosphere–ocean coupling, one may need the best possible streamflow under a given GCM forcing, regardless of its hydrological meaning (or lack of meaning). In this framework, we tried to calibrate RiTHM directly under the LMD GCM forcing, to check if this could override some of the flaws identified above.

An important concern was of course the strong systematic errors of the LMD GCM on total runoff. They prevented riverflow volumes from being accurate (because RiTHM is a conservative RRM), and therefore hindered any adjustment of simulated streamflow to the observed one. Given that the main difference between streamflow and the spatial accumulation of total runoff is the time lag between these two quantities, it was decided to focus the calibration on the correct reproduction of this time lag. Moreover, the time lag between peak runoff and peak discharge was emphasized, since the simulation of floods is expected to have a higher impact on the coupled climate system than that of low flows (related to a smaller freshwater input to oceans). Finally, to limit the degrees of freedom during the calibration (which cannot be precise anyway because of the volume errors), we arbitrarily set $K_i = 0.02\ \mathrm{d}^{-1}$ ($\tau_i = 50$ d), so that only one parameter, namely C_s, controlled the storage within the cells of RiTHM. Under the ISLSCP runoff forcing, $K_i = 0.02\ \mathrm{d}^{-1}$ seemed representative of rivers without important storage in hydraulic annexes (Table 1).

The resulting hydrographs (Fig. 9) agree much better with observed streamflow than the hydrographs simulated by RiTHM with the previous set of parameters (calibrated with the ISLSCP runoff). This is true in all the studied basins, and the strongest improvements address the timing of the hydrograph, as expected. This is clearly shown by the correlation coefficients (Table 3), which are markedly larger than those in Table 2 (RiTHM with GCM runoff and first set of parameters), and are as high as those in Table 1 (RiTHM with the ISLSCP runoff and the corresponding first set of parameters). This timing improvement increases the efficiency of Nash compared to Table 2, but only in the basins where the volume error is not overwhelming (first five in Table 3). This criterion can even exceed the one from Table 1, in the Volga and Amur, but most likely for the wrong reasons.

As shown in Table 3, these improvements are related to important changes in T_c (except in the Danube and Ganges, where the timing was already satisfactory). These changes compensate for errors in time and/or spatial distribution of the runoff forcing,

Table 3
Results of the calibration of RiTHM forced with the GCM runoff in the selected 11 river basins. See Table 1 for explanations

Rivers	T_c (days)	U (m s^{-1})	C_s (mm.d^{-1})	C_s (%)	Nash (–)	ρ (–)
Ob	180	0.48	5	59	0.25	0.76*
Yenisei	60	2.78	10	67	0.38	0.91*
Volga	180	0.19	0	0	0.77	0.56†
Amur	195	0.19	0	0	0.87	0.90*
Mackenzie	540	0.13	0	0	0.47	0.91*
Mississippi	15	2.24	8	75	−10.85	0.81*
Danube	90	0.56	8	77	−31.59	0.96*
Amazon	105	0.50	30	92	−2.68	0.93*
Congo	450	0.11	20	88	−64.41	0.80*
Niger (Malanville)	360	0.15	30	90	−1891.	0.87*
Ganges-Br	90	0.36	15	44	−2.95	0.99*

and lead to velocities that are not always realistic. It is the case for the very low values (smaller than 0.15 m s^{-1} in the Mackenzie and Congo basins) and the much too high values (greater than 2 m s^{-1} in the Yenisei and Mississippi basins). The values of C_s also change, and unrealistically concentrate at the two bounds of the infiltration range, which again compensates for flaws in the runoff forcing. The absence of infiltration helps to sharpen the flood peak in the Volga, Amur and Mackenzie. On the other hand, very high infiltration percentages help to smooth down the hydrograph. As in Section 4.1, the calibration here was manual, and again, it is likely that other combinations of parameters (especially if K_i was allowed to vary) could give similar or better results.

In the Niger basin, simulated streamflow was compared to observations in Malanville instead of Niamey (as in Fig. 8), since Malanville is the closest to the outlet, and therefore best suited for climate-oriented calibration. The overestimation of streamflow is very high (Fig. 9 displays 10 times the observed discharge in Malanville), because of two additive reasons: the overestimation of precipitation and the processes that are neglected in RiTHM, such as storage and flow diversion through the inner delta (Section 4.1.2). The GCM precipitation is correctly phased in the Niger basin (Fig. 10), and we did not detect any anomalous rainfall patterns beside enhanced contrasts. Therefore, precipitation does not explain the very strong increase in T_c compared to the calibration based on the ISLSCP runoff (Table 1). Part of the reason is that, even with the ISLSCP runoff forcing (Fig. 8), peak flow is already too early in Niamey (although to a lesser extent), because the calibration of T_c was based on recessions rather than floods, since they are poorly simulated because of the neglected processes. But the main reason for the earlier flood peak in Malanville, when T_c is not calibrated there, could be a reduction of the river velocity downstream from Niamey (for the part of velocity that does not depend on topography, and is not already accounted for in T_c). This is consistent with the decrease in streamflow (related to velocity) along the inner delta. This shows that RiTHM, with its basin-wide lag parameter T_c, is not sufficiently complex for river basins with heterogeneous river velocities.

5. Discussion and conclusions

We have described a new runoff routing model (RRM) for use in GCMs. This model, RiTHM, which can be seen as an adaptation to the macro-scale of the hydrological model MODCOU (Ledoux et al., 1989), has two main features compared to RRMs previously used in GCMs. The first one is a high spatial resolution ($\simeq 25 \times 25$ km^2), allowing a precise delineation of macro-scale river basins and the capture of sharp topographic contrasts. The second original feature, related to the first one by means of computational cost reduction, is the simplicity of its routing algorithm. The lateral transfer across grid-cells is performed in the surface drainage network only, under the assumption of pure translation. This implies that the transfer from one cell is independent of the transfer from any other cell, and of any possible interaction with the environment (e.g. storage in reservoirs, flooding, or human intake). Therefore, it only depends on topography and a basin-wide parameter, the time of concentration T_c.

Groundwater storage (in the soil, unsaturated zone and aquifers) is accounted for in every cell, where it is controlled by two parameters, C_s and K_i. Groundwater flow between the cells, however, is neglected, under the assumption that there is at least one stream in every 625 km^2 cell to insure the local discharge of groundwater to the river. It would be possible, however, to reintroduce the physically-based description of groundwater fluxes from the hydrological model MODCOU. This would make it possible to simulate the interactions between groundwater and climate, which can be important with respect to long-term climate variations.

In the 11 macro-scale river basins where RiTHM was tested, we showed that this model was easy to calibrate (assuming uniform values of C_s and K_i in each basin), leading to satisfactory results under the realistic ISLSCP runoff forcing (Section 4.1). This exercise was, of course, not a proper validation of the model, since we had no additional observed forcing data to validate the calibration performed in 1987–1988. The ISLSCP II data set (IGPO, 1996; Hall et al., 2002) providing a meteorological forcing suitable for LSMs over the period 1986–1995, could be very helpful in this context.

Under the ISLSCP runoff forcing, the main flaws in the simulated hydrographs were likely related to hydraulic processes that were neglected in RiTHM, namely the storage in reservoirs (natural or artificial), and the diversion of riverflow because of flooding or irrigation, as discussed in the cases of the Niger and Congo (Section 4.1.2). A consequence of this result is that SECHIBA, the LSM used to simulate the runoff forcing, was not a factor affecting the quality of simulated hydrographs, which validates this LSM. Exceptions were found, however, in high-latitudes river basins, which suggests that snow processes are too simplistic in SECHIBA.

It is interesting at this point to compare these results with the ones by Oki et al. (1999). They forced their linear RRM, called STRIP, with runoff data sets that are very similar to the one we used above (simulated by 11 LSMs under the ISLSCP meteorological forcing used to force the LSM SECHIBA in our study). In the basins where the comparison is possible (Amazon, Mississippi and Mackenzie), the hydrographs simulated by RiTHM are more realistic than the ones in Oki et al. (1999). SECHIBA might respond better than the LSMs tested there, but the main differences seem related to the RRMs. STRIP does not account for infiltration, which prevents a good reproduction of low flows. But the main problems with STRIP, especially in the Amazon and Mississippi, are timing problems, which stem directly from the assumption of globally constant velocity ($0.5\ m^{-1}$). This comparison clearly demonstrates the importance of calibration.

Still using the parameters calibrated with the ISLSCP runoff, RiTHM was also forced with runoff from the LMD GCM. An important result, although not new (Miller et al., 1994; Arora and Boer, 1999), was that the quality of simulated streamflow was strongly limited by the quality of GCM simulated precipitation. Any error in this term, with respect to total amount, seasonal variations or, as importantly, spatial distribution (see the case of the Congo, at the end of Section 4.2.1), affected total runoff (RiTHM's input), and therefore induced errors in simulated streamflow. More generally, any inaccuracy in the GCM climate that could affect the simulation of runoff should degrade the simulation of streamflow. The influence of the temperature bias at high latitude over the sequence snowmelt/runoff/streamflow (Section 4.2.1) was very illustrative in this regard.

We also calibrated RiTHM directly under the GCM-runoff forcing, which markedly improved the quality of the simulated hydrographs compared to the previous ones. The main improvement addressed the timing of hydrographs, because RiTHM is a conservative RRM and cannot compensate for volume errors. One should be aware, however, that adequate performances using GCM runoff can happen for the wrong reasons (one error masking another one), as illustrated in the case of the Amur (Section 4.2.2).

Finally, this work demonstrated the suitability of RiTHM for the two main roles of a macro-scale RRM, which are the assessment of modeled runoff against observed discharge, and the simulation of discharge from GCM runoff in climate studies. But the main reason for the good performances of RiTHM in both types of exercises is the calibration of its parameters rather than some intrinsic quality of the model. Most RRMs for GCMs, however, use a priori parameters. We argue that, if a RRM and its parameters are not calibrated, or validated, in plausible situations, then this model cannot help to evaluate a runoff forcing, since it is not possible to quantify the contribution of the RRM to the overall error. And if the runoff forcing is erroneous, as it is the case in most GCMs, then the simulated discharge will be too. In such a context, calibrating the parameters accounting for the delay between runoff and discharge (which is the main role of RRMs) can prove interesting for climate studies. From a hydrological point of view, however, this must remain a temporary solution, until the simulated water cycle improves in GCMs.

Acknowledgements

We thank the reviewers for their helpful comments on the manuscript. Comments from Balazs M. Fekete were especially insightful. We are also very grateful to Daniel Conley for his careful correction of this paper's English. Most observed discharge data were provided by Taikan Oki (Laboratory for Hydrology and Water Resources, University of Tokyo, Japan), and by the Global Runoff Data Centre (D-56002 Koblenz, Germany). The GCM simulation used in

this study was performed using the computational facilities of the Institut du Développement et des Ressources en Informatique Scientifique (CNRS, France).

References

Ambroise, B., Perrin, J.L., Reutenauer, D., 1995. Multicriterion validation of a semidistributed conceptual model of the water cycle in the Fecht catchment. Water Resour. Res. 31 (6), 1467–1481.

Arora, V., Boer, G., 1999. A variable velocity flow routing algorithm for GCMs. J. Geophys. Res. 104 (D24), 30965–30979.

Avissar, R., Pielke, R., 1989. A parametrization of heterogeneous land surfaces for atmospheric numerical models and its impact on regional meteorology. Mon. Weather Rev. 117, 2113–2136.

Boukerma, B. 1987. Modélisation des écoulements superficiels et souterrains dans le Sud-Ouest de la France : approche du bilan hydrique. Thèse de l'Ecole Nationale Supérieure des Mines de Paris, Fontainebleau, France.

Campos, E., Lentini, C., Miller, J., Piola, A., 1999. Interannual variability of the sea surface temperature in the South Brazil Bight. Geophys. Res. Lett. 26, 2061–2064.

Cavazzi, C., 1995. Exploitation d'un modèle numérique de terrain pour l'aide à la mise en place d'un modèle hydrologique distribué. DEA d'Hydrologie, Université Paris 6, Paris, France.

Choisnel, E.M., Jourdain, S.V., Jacquart, C.J., 1995. Climatological evaluation of some fluxes of the surface energy and soil water balances over France. Ann. Geophys. 13, 666–674.

Coe, M.T., 1998. A linked global model of terrestrial hydrologic processes: Simulation of modern rivers, lakes, wetlands. J. Geophys. Res. 103 (D8), 8885–8899.

Coe, M.T., 2000. Modeling terrestrial hydrological systems at the continental scale: testing the accuracy of an atmospheric GCM. J. Clim. 13, 686–704.

Dingman, S., 1994. Physical Hydrology, Prentice-Hall, Upper Saddle River, NJ.

Dirmeyer, P., Dolman, H., 1998. Global Soil Wetness Project: Preliminary Report on the Pilot Phase, IGPO Publication Series 29.

Ducharne, A., 1997. Le cycle de l'eau: modélisation de l'hydrologie continentale, étude de ses interactions avec le climat. Thèse de Doctorat de l'Université Paris 6, Paris, France.

Ducharne, A., Laval, K., 2000. Influence of the realistic description of soil water-holding capacity on the global water cycle in a GCM. J. Clim. 13, 4393–4413.

Ducharne, A., Laval, K., Polcher, J., 1998. Sensitivity of the hydrological cycle to the parametrization of soil hydrology in a GCM. Clim. Dyn. 14, 307–327.

Ducoudré, N., Laval, K., Perrier, A., 1993. SECHIBA, a new set of parametrizations of the hydrologic exchanges at the land/atmosphere interface within the LMD atmospheric general circulation model. J. Clim. 6 (2), 248–273.

Dümenil, L., Todini, E., 1992. A rainfall-runoff scheme for use in the Hamburg climate model. In: O'Kane, J., (Ed.), Advances in Theoretical Hydrology, A Tribute to James Dooge, European Geophysical Society Series in Hydrological Sciences, vol. 1. Elsevier, Amsterdam, pp. 129–157.

Edwards, M.O., 1989. Global Gridded Elevation and Bathymetry (ETOPO5), Digital Raster Data on a 5-minute Geographic (latxlon) 2160 × 4320 (centroid-registered) grid, NOAA National Geophysical Data Center, Boulder CO.

Fekete, B.M., Vörösmarty, C.J., Lammers, R.B., 2001. Scaling gridded river networks for macroscale hydrology: development, analysis, control of error. Water Resour. Res. 37, 1955–1967.

Gates, W.L., 1992. AMIP, the atmospheric model intercomparison project. Bull. Am. Meteorol. Soc. 73, 1962–1970.

Gille, E., 1985. Etude hydrologique des bassins de la Meuse et de la Moselle. Thèse de l'Ecole Nationale Supérieure des Mines de Paris, Fontainebleau, France.

Golaz, C., 1999. Modélisation hydrologique à l'échelle régionale appliquée au bassin du Rhône. Comparaison de deux modes de calcul des bilans hydriques de surface et étude de sensibilité à une perturbation des forçages climatiques. Thèse de Doctorat de l'Ecole des Mines de Paris, Fontainebleau, France.

Gomez, E., Ledoux, E., Mary, B., 1999. The approach for modelling water and nitrogen production and transfer in the Seine river basin; structure of the hydrological model. Technical report, Programme PIREN-Seine, CNRS/Universit, Paris 6, Paris, France. pp. 1–13 (in French).

Grabs, W., DeCooet, T., Pauler, J., 1996. Freshwater fluxes from the continents into the world oceans based on data of the global runoff data base. Technical Report 10, Global Runoff Data Center, Koblenz, Germany.

Habets, F., Etchevers, P., Golaz, C., Leblois, E., Ledoux, E., Martin, E., Noilhan, J., Ottlé, C., 1999. Simulation of the water budget and the river flows of the Rhone basin. J. Geophys. Res. 104(D24), 31145–31172.

Hagemann, S., Dümenil, L., 1998. A parametrization of the lateral waterflow for the global scale. Clim. Dyn. 14, 17–31.

Hall, F., Meeson, B., Los, S., Steyaert, L., deColstoun, E., Landis, D. 2002. Islscp initiative ii. NASA. DVD/CD-ROM. Complementary information on http://islscp2.sesda.com/ISLSCP2_1/html_pages/islscp2_home.html.

IGPO, 1996. International Satellite Land-Surface Climatology Project (ISLSCP) Initiative II: Global data sets 1986–1995, IGPO Publication Series, vol. 17., 68 pp.

Koster, R.D., Suarez, M., Ducharne, A., Stieglitz, M., Kumar, P., 2000. A catchment-based approach to modeling land surface processes in a GCM—part 1: model structure. J. Geophys. Res. 105 (D20), 24809–24822.

Koster, R.D., Suarez, M.J., 1992. Modeling the land surface boundary in climate models as a composite of independants vegetation stands. J. Geophys. Res. 97 (D3), 2697–2715.

LeTreut, H., Li, Z.-X., 1991. Sensitivity of an atmospheric general circulation model to prescribed SST changes: feedback effects associated with the simulation of cloud optical properties. Clim. Dyn. 5, 175–187.

Leblois, E., Sauquet, E., 2000. Grid elevation models in hydrology—Part 1: principles and literature review; Part 2:

HydroDem user's manual. Technical note, Cemagref, Lyon, France. 80 pp (in French).

Ledoux, E., 1980. Modélisation intégrée des écoulements de surface et des écoulements souterrains sur un bassin hydrologique. Thèse de Docteur-Ingénieur, Ecole Nationale Supérieure des Mines de Paris et Université Paris 6, Paris, France.

Ledoux, E., Girard, G., deMarsily, G., Villeneuve, J.-P., Deschenes, J., 1989. Spatially distributed modeling : conceptual approach, coupling surface water and groundwater. In: Morel-Seytoux, H.J., (Ed.), Unsaturated Flow in Hydrologic Modeling—Theory and Practice, NATO ASI Ser C, vol. 275. Kluwer Academic, Norwell, Mass, pp. 435–454.

Legates, D.R., Willmott, C.J., 1990. Mean seasonal and spatial variability in gauge-corrected, global precipitation. Int. J. Climatol. 10, 111–127.

Liang, X., Lettenmaier, D., Wood, E., Burges, S., 1994. A simple hydrologically based model of land surface water and energy fluxes for general circulation models. J. Geophys. Res. 99 (D7), 14415–14428.

Liston, G.E., Sud, C., Wood, E.F., 1994. Evaluating GCM land surface hydrology parameterizations by computing river discharges using a runoff routing model : application to the Mississipi basin. J. Appl. Meteorol. 33, 394–405.

Maidment, D.R., 1996. GIS and hydrologic modeling : an assessment of progress. Paper presented at the Third International Conference on GIS and Environmental Modeling, January 22–26, 1996, Santa Fe, New Mexico, USA. Available on http://www.ce.utexas.edu/prof/maidment/gishydro/meetings/santafe/santafe.htm.

Miller, J.R., Russel, G.L., Caliri, G., 1994. Continental-scale river flow in climate models. J. Clim. 7, 914–928.

Murtugudde, R., 1998. The role of river discharges in the interannual variability of the atlantic ocean between 1958–1998. Invited presentation at the TAO Implementation Panel Meeting. (Abidjan, Ivory Coast, November, 1998).

Mysak, L.A., Manak, D.K., Marsden, R.F., 1990. Sea-ice anomalies observed in the greenland and labrador seas during 1901–1984 and relation to an interdecadal Artic climate cycle. Clim. Dyn. 5, 111–133.

Nash, J.E., 1959. Systematic determination of unit hydrograph parameters. J. Geophys. Res. 61 (1).

Nash, J.E., Sutcliffe, J.V., 1970. River flow forecasting through conceptual models. Part I : a discussion of principles. J. Hydrol. 10, 282–290.

Oki, T., Nishimura, T., Dirmeyer, P., 1999. Validating land surface models by runoff in major river basins of the globe using total runoff integrating pathways (TRIP). J. Meteor. Soc. Japan 77, 235–255.

Oki, T., Sud, Y.C., 1998. Design of Total Runoff Integrating Pathways (TRIP) A global river channel network. Earth Interact. 2 (1).

Olivera, F., Maidment, D., 1999. Geographic information systems GIS-based spatially distributed model for runoff routing. Water Resour. Res. 35 (4), 1155–1164.

Pilgrim, D.H., Cordery, I., 1992. Flood runoff. In: Maidment, D.R., (Ed.), Handbook of Hydrology, McGraw-Hill, New York.

Rawls, W.J., Ahuja, L.R., Brabensiek, D.L., Shirmohammadi, A., 1992. Infiltration and soil water movement. In: Maidment, D.R., (Ed.), Handbook of Hydrology, McGraw-Hill, New York.

Renssen, H., Knoop, J., 2000. A global river routing network for use in hydrological modeling. J. Hydrol. 230, 230–243.

Rowntree, P.R., Lean, J., 1994. Validation of hydrological schemes for climate models against catchment data. J. Hydrol. 155, 301–323.

Sadourny, R., Laval, K., 1984. January and July performance of the LMD general circulation model. In: Berger, A.L., Nicolis, C. (Eds.), New Perspectives in Climate Modelling, Elsevier Science Publishers, Amsterdam, pp. 173–197.

Saghafian, B., Julien, P.Y., Rajaie, H., 2002. Runoff hydrograph simulation based on time variable isochrone technique. J. Hydrol. 261, 193–203.

Sellers, P., Meeson, B.W., Closs, J., Collatz, J., Corprew, F., Dazlich, D., Hall, F.G., Kerr, Y., Koster, R., Los, S., Mitchell, K., McManus, J., Myers, D., Sun, K.J., Try, P., 1996. The ISLSCP inititative I global data sets: surface boundary conditions and atmospheric forcings for land–atmosphere studies. Bull. Am. Meteor. Soc., 77.

UNESCO, 1993. Discharge of selected rivers of the world. Vol. 2. Part 2. Mean monthly and extreme discharges (1965–1984). Technical report, UNESCO Press, Paris, France. 288 pp.

Vörösmarty, C., Fekete, B., Tucker, B., 1996. River Discharge Database, Version 1.0 (RivDIS v1.0), Volumes 0 through 6. A contribution to IHP-V Theme 1. Technical documents in hydrology series, UNESCO, Paris, France.

Vörösmarty, C.J., Moore, B., Grace, A.L., Gildea, M.P., Melillo, J.M., Peterson, B.J., Rastetter, E.B., Steudler, P.A., 1989. Continental scale models of water balance and fluvial transport : an application to South America. Global Biogeochem. Cycles 3 (3), 241–265.

Weller, R., 1998. The hydrological cycle linking the ocean and atmosphere to land. Invited presentation at the AGU Fall Meeting 1998 (San Francisco, CA, USA).

Wood, E., Lettenmaier, D., Zartarian, V., 1992. A land-surface hydrology parameterization with subgrid variability for general circulation models. J. Geophys. Res. 97 (D3), 2717–2728.